

## SAND DYNAMICS ALONG THE BELGIAN COAST BASED ON AIRBORNE HYPERSPECTRAL DATA AND LIDAR DATA

*Bart Deronde, Rik Houthuys, Sindy Sterckx, Walter Debruyn and Dirk Fransaer*

Flemish Institute for Technological Research, Remote Sensing and Atmospheric Processes,  
Mol, Belgium; [bart.deronde\(at\)vito.be](mailto:bart.deronde(at)vito.be)

### ABSTRACT

The goal of this project was to explore the possibilities of airborne hyperspectral data and airborne lidar data to study sand dynamics on the Belgian backshore and foreshore. The Belgian coast is formed by a sandy strip at the southern edge of the North Sea Basin which is commonly known as the Southern Bight. Since the beach is prone to structural and occasional erosion, it is very important to obtain a better understanding of the processes controlling it. The combination of multi-temporal hyperspectral data and lidar data provides a suitable tool for follow-up of the Belgian coastline, and sandy coastlines in general. Hyperspectral imagery generates a reflectance spectrum for each pixel in the image. The shape of this spectrum is influenced by the composition of the topsoil of the beach, being mainly the mineralogical composition and the grain size. A Spectral Angle Mapper (SAM) algorithm was used to perform a supervised classification of the hyperspectral images in order to distinguish between different sand types. Digital terrain models (DTM's) with a mean vertical accuracy of 5 cm were generated from lidar data. By differencing a DTM from September 2000 and one from September 2001 a map with sedimentation and erosion zones was generated. By combining the erosion/sedimentation map with the classified hyperspectral images, dating from August 2000 and August 2001, an appropriate and cost-effective method was found for studying the processes of sand transport along the Belgian coastline.

**Keywords:** imaging spectroscopy, hyperspectral, lidar, coastal zone management

### INTRODUCTION

The Belgian Coast extends over about 65 km between De Panne in the West and Knokke-Heist in the East; see Figure 1. From a geological point of view this coastline is part of the 'Flemish coastal plain', a depositional system at the southern edge of the North Sea Basin. The actual coastline developed during the Holocene and is believed to have been formed by sand supplied naturally from the shelf (1,2). A detailed description of the geological history of the Belgian coast can be found in Rottier and Arnoldus (3). Since the Middle Ages, man has strived to keep the coastline at its position. At present, more than 50 % of the coast length suffers from erosion. A sustainable management of the coastline needs permanent attention and both hard and soft defence works (4).

Today, the coastline is formed by a sandy beach barrier which, at low tide, is more than one kilometre wide west of De Panne. Eastwards the beach barrier narrows to 300-400 m at low tide in Knokke. The median diameter of the sand grains varies between 200 and 350 µm and the grains are almost entirely constituted of quartz.

Since the beach is of major economic importance to Belgium and since it is part of the natural defence protecting the polders against flooding, it is very important to get a better understanding of the processes which control the beach. The economic and social importance of the coastal zone as well as the challenges for the application of remote sensing in these areas are described by Cracknell (5). One way -among others- of gaining insight into the coastal dynamics is the follow-up

of the beach by airborne hyperspectral observations and by airborne lidar<sup>1</sup> measurements (6). The high spatial resolution of airborne imagery makes these data well suited for coastal applications in contrast to spaceborne data which have generally lower spatial resolutions. This is the main reason why in the past decades remote sensing of coastal areas remained less successful than in other areas - meteorology, open oceans, and land. The first airborne data which proved to be suited for coastal studies were aerial photos. Later on, with the introduction of airborne digital cameras, laserscanners, and hyperspectral scanners the possibilities increased rapidly.

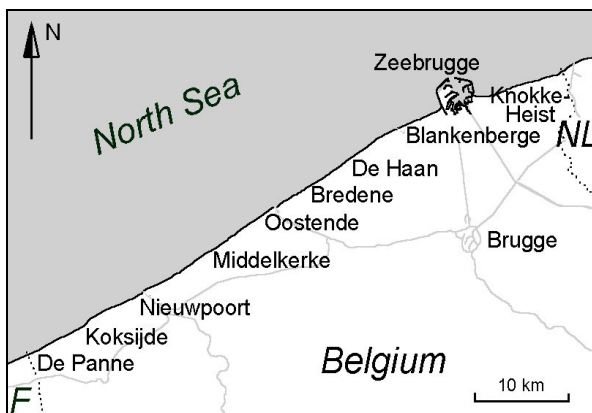


Figure 1: Situation map of the study area.

## METHODS

The dynamics of the beach is studied by using a method which makes it possible to distinguish between different sand types by means of airborne spectroscopy. The mineralogical composition, the granulometric properties, the micro topography, and the soil moisture of the topsoil of the beach influences the reflected sunlight, resulting in a unique reflectance spectrum for each ground point. Airborne spectroscopy is essentially based on classical spectroscopy but adds an imaging component to it; there is a reflectance spectrum for each pixel in the image (7).

On August 23, 2000 a first flight over the entire coast was performed with a CASI-2 sensor measuring the reflected light in a 545 nm spectral range configured between 400 and 1000 nm. The original spatial resolution of the pixels after acquisition was 1 m across-track by 2.2 m along-track. These were resampled with a bi-linear resampling algorithm to 2 m by 2 m pixels. The geometrically and radiometrically calibrated data were corrected for atmospheric influences using ATCOR4 which is based on the radiometric transfer model MODTRAN 4 (8). Simultaneously with the flight differential GPS measurements, sun-photometer measurements and reflectance measurements were performed. The differential GPS is used in combination with the attitude data (i.e. roll, pitch and yaw) of the aircraft to georeference the data as accurately as possible, while the data collected with the sunphotometer and the reflectance measurements were used in the atmospheric correction. The positional accuracy after the geometric correction is in general 1 to 2 pixels. On August 27, 2001 a second acquisition was performed yielding pixels of ¼ m which were in the same way transformed to 2 m by 2 m pixels. In both cases the CASI-2 was set in enhanced spectral mode measuring the reflected light in 96 spectral bands. Due to the poor radiometric quality of the data and the absorption by water vapour the last 13 bands of the acquisition of 2000 had to be eliminated; for the 2001 data the first 19 bands were also unusable. Hence, the analysis was performed on 83 and 64 bands respectively for the data of 2000 and 2001.

After the geometric, radiometric and atmospheric calibration the hyperspectral data were normalised. This step was necessary in order to compare wet to dry spectra. The reflectance of wet sam-

<sup>1</sup> LIDAR is the acronym for Light Detection And Ranging.

ples is much lower than the one of dry samples. Since the flight was performed at low tide a normalisation was absolutely necessary to be able to compare the reflectance curves from all samples over the beach, both backshore and foreshore. Figure 2 illustrates that the spectral reflectance curves of two different samples, regardless of whether they are in dry or wet state, are more similar than the wet and dry state curves of one sample.

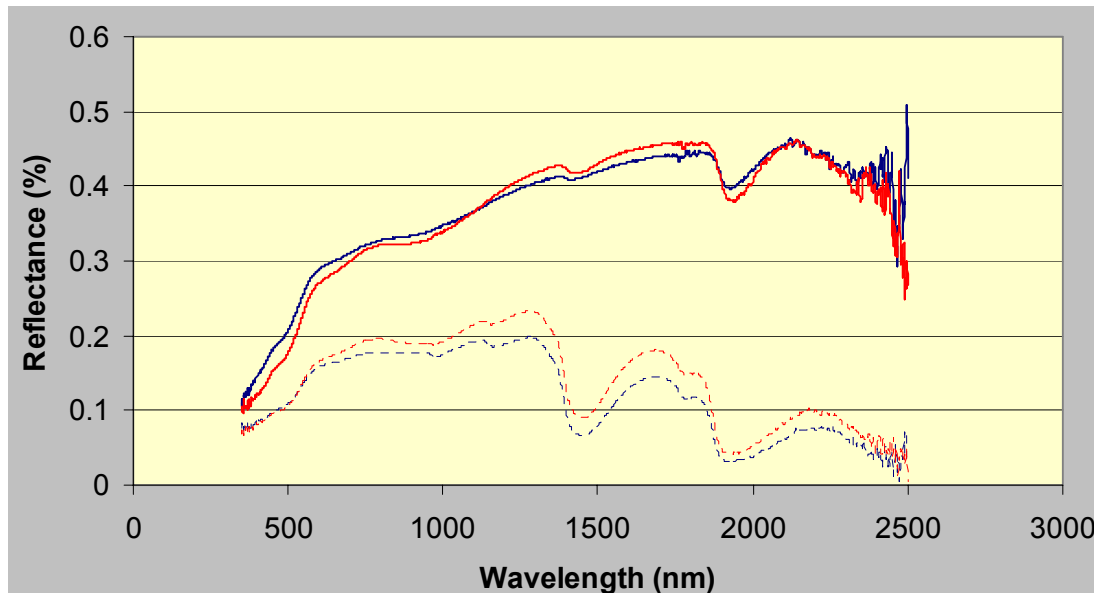


Figure 2: Spectral reflectance measured between 450 and 2500 nm with an ASD (Fieldspec Pro Fr) spectroradiometer. The thin lines are the spectra for wet, saturated samples and the thick lines for dry spectra. Blue and red represent two arbitrary spectra.

In Figure 3 the principle of normalization is illustrated. For each wavelength a factor  $F_\lambda$  is calculated which gives the ratio between the moving average through a theoretical smooth curve with high reflectance and the original but smoothed curve.

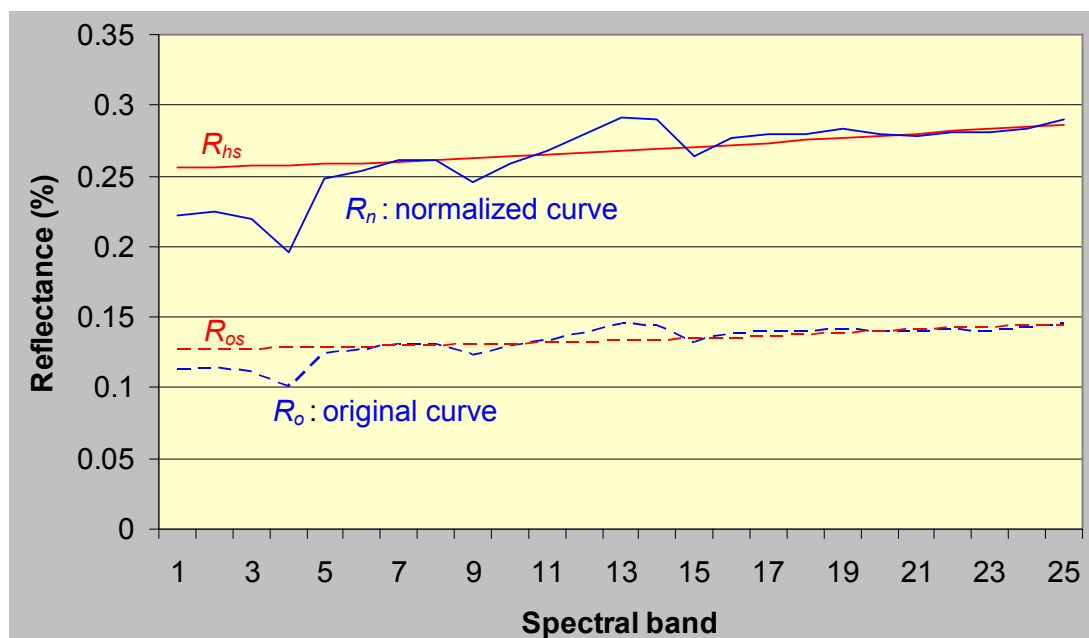


Figure 3: Principle of the normalisation used. The dashed blue curve is the original spectral signal recorded by the CASI-2 sensor. The full blue line is the normalised spectrum 'lifted' to the level of the full red line (all spectra are lifted to this level). The dashed red line is a moving average through the dotted blue line.

The resulting normalised reflectance,  $R_{n\lambda}$ , is calculated as follows:

$$R_{n\lambda} = [(R_o - R_{os}) \cdot F_\lambda + R_{hs}]_\lambda \quad (1)$$

with

$$F_\lambda = R_{hs} / R_{os} \quad (2)$$

Note that this method preserves the shape of the curve while the absolute values of the reflectance are lost.

After the normalisation the first derivative of the spectra was calculated in order to accentuate the small absorption features present in the data.

Finally, an unsupervised SAM (Spectral Angle Mapper) algorithm was applied to classify the pixels. SAM considers each spectrum as an N-dimensional vector, where N is the number of bands, and compares this vector with pre-defined library spectra (9). The result of this processing chain is a classified map with eight distinct sand classes.

The second part of the project is based on lidar data. In aerial laserscanning the scanner deflects a laser beam across the flight line and detects its reflection, so that a swath of ground along the flight line is sampled along a zig-zag line. The distance to the earth's surface is determined by measuring the pulse return time. The physical attitude, i.e. the position and orientation of the sensor is calculated from d-GPS and INS (Inertial Navigation System) data. In combination with the scan angle, the 3D position of each laser beam spot on the surface can be determined. In this case an ALTM 1225 system designed by Optech Inc. was used. This is an infrared laser operating at a wavelength of 1047 nm with a pulse frequency of 25.000 Hz. The point density of the raw data is 1 point every 4 m<sup>2</sup>. Elements which do not belong to the earth's surface, e.g. beach cabins, were eliminated using a morphological filter. After the filtering the point density is reduced to 1 point every 16 m<sup>2</sup>. To verify the accuracy of the DTM, 10 reference sites were mapped autonomously. The individual points were not exactly at the same locations as the DTM points, but all reference sites were selected on flat surfaces, e.g. flat and wide seawall tops. Hence, by spatial interpolation of the laserscan data, it was possible to calculate the height at the points that were measured by the surveyor. This verification proved a mean height accuracy of 5 cm (with a standard deviation of 7 cm).

The first laserscanning was performed on September 11, 2000, the second on September 28, 2001. Hence, there is one month of time lag between the hyperspectral recordings and the laserscanning caused by technical problems with the laserscanner. This was not an ideal situation but luckily, in the month between both acquisitions no heavy weather conditions were reported so that we can assume that there was no major change in the state of the beach between both dates. By subtracting the 2000 DTM from the 2001 DTM, a map with erosion and sedimentation zones was derived. Hence the laserscan data give quantitative information on the morphological changes, while the hyperspectral data indicate the types of sand which were transported (10,11).

## RESULTS

### Hyperspectral data analysis

Since the SAM classification is a statistical clustering method, different levels of classification, i.e. different number of classes, can be obtained. It was found that the sand occurring along the Belgian coast can optimally be divided into eight classes according to their reflectance spectrum. This number can be discussed; based on field knowledge eight classes were considered as a good number to study the sand dynamics on the scale of the Belgian coast. Less classes would hide certain processes and more classes would needlessly complicate the patterns. But for studies on another scale it may be better to choose another number of classes.

The supervised classification is based on library spectra which were defined after extensively studying the hyperspectral cubes and by using years of field experience. Along the entire coast regions with a specific type of sand were marked on the hyperspectral images. The mean spectral signatures for these regions were used as library spectra.

Figure 4 illustrates a classification of the beach near Zeebrugge; in the west the image is bounded by the pier of Blankenberge, in the east by the harbour of Zeebrugge. Eastward of the Pier of Blankenberge, an artificial beach nourishment zone stands out. Between October 1998 and April 1999, almost 500 000 m<sup>3</sup> of sea sand was put on the backshore. The sea sand is coarser than the original sand (class 5), contains a large amount of shells and even some gravel. Because of its different composition it can spectrally be distinguished from other sand types. There are two classes with similar colour; orange (class 7) and light-red (class 8). Both correspond to relatively coarse-grained sand containing shell fragments. Classes 7 and 8 are also present in patches east of the nourished area. Their presence is indicative for erosion at the nourishment site and eastward longitudinal transport. It is the same transport that has caused the very wide beach at Zeebrugge, just west of the harbour dam. The beach accreted primarily after the completion of the harbour dam (late 1970s), but the sand accumulation is going on to the present day. The brown class (2) corresponds to fine grained and slightly muddy sand; it is present on the lowest parts of the beach in the swales. At the eastern lee of the Pier of Blankenberge the same type of sand is found. The green and grey classes (3 and 4) represent relatively fine sand types on the intertidal part of the beach. Class 6 is a rare class, often found along the high water line and consisting of coarse-grained sand. It occurs sometimes together with classes 7 and 8.

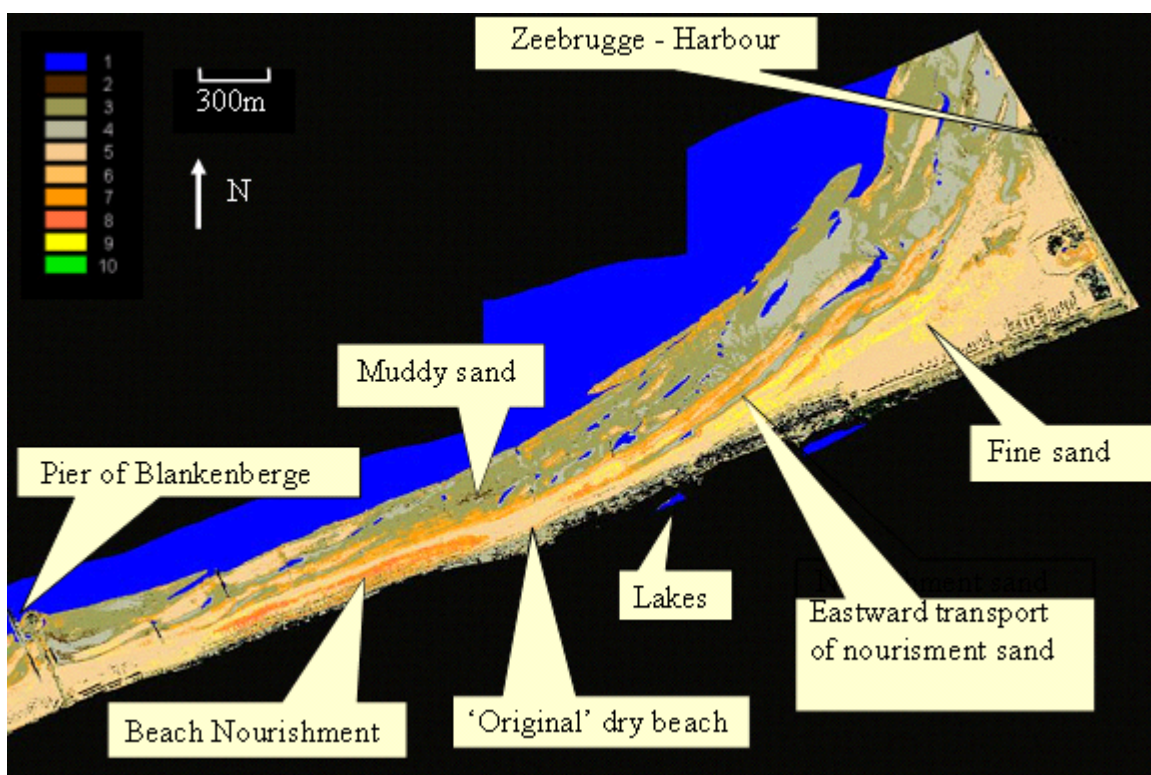


*Figure 4: Classified image (2000 survey) of the beach between Blankenberge and Zeebrugge derived by SAM classification. Eight different sand types can be distinguished. Class number 1 is water, number 10 is vegetation and classes 2 to 9 represent the eight sand types.*

#### Lidar data analysis

Figure 5 is a 3D-elevation map of the 2000 DTM near Oostduinkerke. One can see clearly the breaker banks, swales and rip channels in blue and purple on the foreshore (lower part of the scene). The red rectangular shapes are high buildings in the town of Oostduinkerke. The yellow parts bordering the beach and occurring in some inland areas are mainly dunes. The highest dunes in this area are approximately 20m (above the mean low water level in Oostende).

When subtracting the 2000 DTM from the 2001 DTM one generates a height difference map in which elevation loss corresponds to erosion and positive elevation changes indicate sedimentation. Since the vertical accuracy of the DTM is very high it is possible to calculate the amounts of transported sand with high precision.

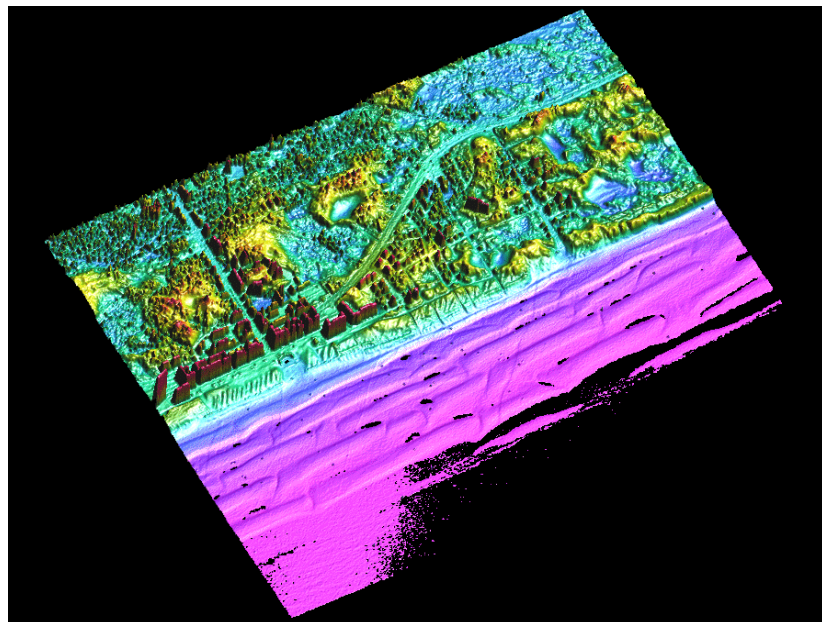


Figure 5: 3D representation of a DTM recorded on September 11, 2000 near Oostduinkerke (Koksijde).

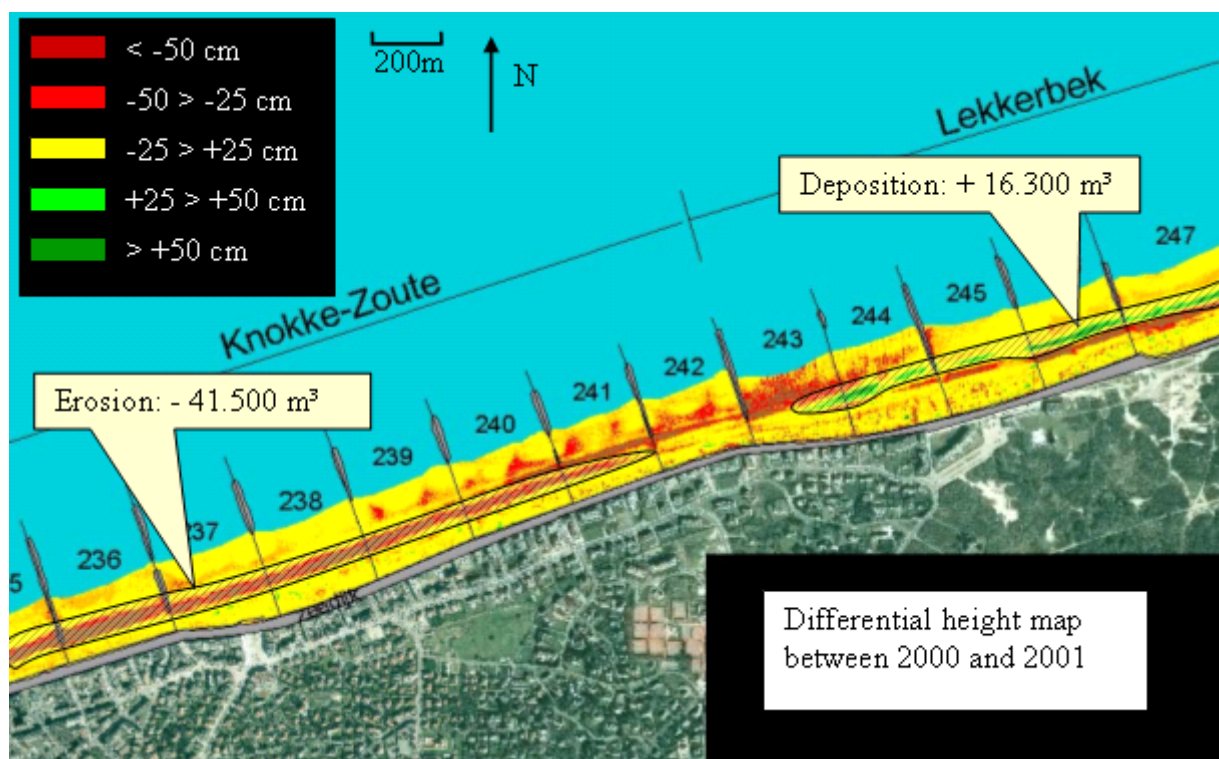


Figure 6: Erosion/sedimentation map of the area between Knokke and the Dutch border. The red zones were subject to erosion, the green zones were characterized by sedimentation, while no important erosion or sedimentation was measured in the yellow zones. Colours are applied in 25 cm height difference classes. Note that the major erosion took place at the seaward side of the beach nourishment zone (shaded area on the left of the image). The shaded polygon on the right is a zone with deposition. The numbers label beach survey sections.

Figure 6 shows the erosion/sedimentation map for Knokke. The red zones were subject to erosion, the green zones were characterized by sedimentation, while no important erosion or sedimentation was measured in the yellow zones. The shaded polygon in front of the urban area of Knokke is a zone where an artificial beach nourishment was carried out in 1999. It is clear that the major ero-

sion took place at the seaward side of this zone; 41 500 m<sup>3</sup> sand were eroded in one year. More to the east, erosion is seen along the high water mark, while a sedimentation zone is visible just under the high water mark (16 300 m<sup>3</sup>). These volumes will have to be confirmed with new data but they are in the same order of magnitude as earlier calculations (4).

### Combination of hyperspectral and LIDAR DATA

The erosion/sedimentation maps (ES-maps) get a meaningful interpretation if they are combined with the sand type maps, established using the hyperspectral recordings. The ES-maps give pixel wise height changes, and the classifications of 2000 and 2001 provide for each pixel the sand type occurring on these two dates. However, this is purely static information. It becomes more interesting when the ES maps are combined with the two classifications because then it is possible to see whether erosion or sedimentation was accompanied by a class change. For instance, in Figure 7 one can see that the eroded sand in front of the Knokke urban area is beach nourishment sand (orange class) and that the sedimentation area eastward of Knokke contains the same type of sand. This is an indication that the sand eroded at the nourishment zone, has been deposited in the accretion area of Figure 6. The volume differences (Figure 6) show that only part of the eroded sand has been deposited in neighbouring areas.

This example clearly shows that combining both types of data opens possibilities for a better understanding of the transport processes along the beach. Successive recordings in the years to come will reveal more dynamics. If the nourishment sand in Knokke is progressively transported towards the east, as is sometimes put forward, new surveys will unambiguously show this process, and will allow to quantify it.

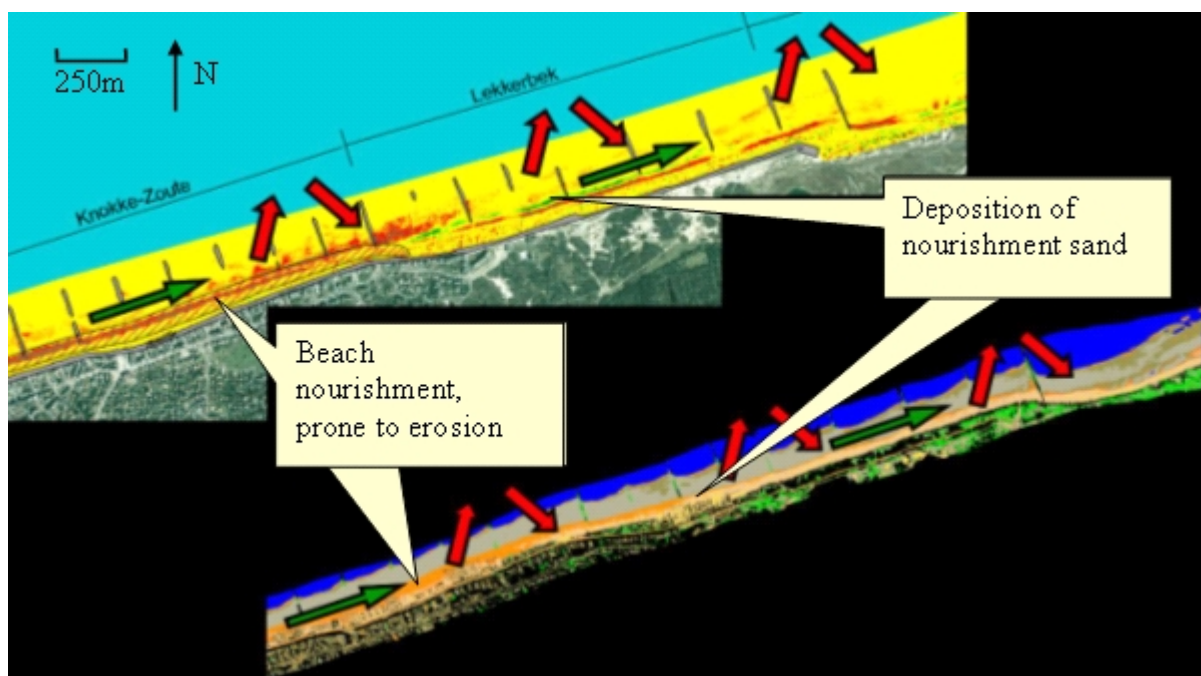


*Figure 7: Combination of a classified image of the beach between Knokke and the Dutch border (below) and a differential height map (above); acquisition in 2001. Combining both leads to more insight in the processes of sand transport on the backshore and foreshore. The shaded polygon indicates an area where an artificial beach nourishment has been executed. The red and green arrows represent the longitudinal and transversal transport mechanisms.*

### CONCLUSIONS

A new method to study beach morphodynamics is presented in this article. The method consists of performing (quasi) simultaneous airborne hyperspectral and LIDAR recordings of the beach at low tide. The hyperspectral recordings were classified into meaningful sand type classes. The laser-scan data was used to make accurate DTM's. Joint interpretation of two successive sand type

surveys and terrain elevation surveys allowed the first conclusions to be drawn about the resultant sand transport processes. They confirm the general theory of eastward transport by longitudinal and transversal movements and erosion at the seaward side of beach nourishment zones. In Knokke 41 500 m<sup>3</sup> of nourished sand was eroded between September 2000 and September 2001 at the seaward side of the nourishment zone, while 16 300 m<sup>3</sup> of the same type of sand were deposited eastward along the high water line. Hence, a large amount of the eroded sand was not deposited between the low water line and the dune foot again, resulting in a net erosion. A third airborne campaign is necessary to confirm the first findings and to analyse the transport processes more in more detail. This will be performed in the near future. One practical application of the better morphological understanding is the optimisation of major soft and hard coastal defence work programmes.

## ACKNOWLEDGEMENT

This project is sponsored by the Flemish Government', Department Environment & Infrastructure, Administration Waterways & Seaways, Section Waterways Coast. We thank Ir. Peter De Wolf and Ir. Toon Verwaest for the good co-operation.

## REFERENCES

- 1 Baeteman C & P-Y Declercq, 2002. A synthesis of early and middle Holocene coastal changes in the western Belgian lowlands. Belg. Tijdschrift voor Geografie, 2: 77-107
- 2 Beets D J & A J F van der Spek, 2000. The Holocene evolution of the barrier and the back-barrier basins of Belgium and the Netherlands as a function of late Weichselian morphology, relative sea-level rise and sediment supply. Geologie en Mijnbouw, 79 (1): 3-16.
- 3 Rottier H & H Arnoldus, 1984. De vlaamse kustvlakte van Calais tot Saeftinge. Lannoo (Tielt), 208 pp.
- 4 Hillen R & Verhagen H J (eds.), 1993. Coastlines of the Southern North Sea, American Society of Civil Engineers (New York) 363 pp.
- 5 Cracknell A P, 1999. Remote sensing techniques in estuaries and coastal zones-an update. International Journal of Remote Sensing, 19(3): 485-496
- 6 Wensink G J, Calkoen C J, Hesselmans G H F M, Vogelzang J, Kokke J M M, Greidanus H S F, Roelvink J A, Rocher de Grimal V & Gerritsen H, 1999. Coastal sediment transport assessment using SAR imagery (C-Star), Beleidscommissie Remote Sensing, USP-2 report 99-18, 30 pp.
- 7 Ben-Dor E, Patkin K, Banin A & Karnieli A, 2002. Mapping of several soil properties using DAIS-7915 hyperspectral scanner data - a case study over clayey soils in Israel. International Journal of Remote Sensing, 23(6): 1043-1062
- 8 Richter R & Schläpfer D, 2002. Geo-atmospheric processing of airborne imaging spectrometry data. Part 2: Atmospheric/Topographic Correction. International Journal of Remote Sensing, 23(13): 2631-2649
- 9 Landgrebe D A, 2003. Signal theory methods in multippectral remote sensing. Wiley Series in Remote Sensing and Image Processing (New Jersey) 508 pp.
- 10 Green D R & King S D, 1999. Remote sensing: an information source for better coastal zone management. Proceedings of the Fourth International Airborne Remote Sensing Conference and Exhibition (Ottawa) 21-24 June 1999, II/470-II/477
- 11 Pernetta J C & Milliman J D, 1995. Land-ocean interactions in the coastal zone. Implementation plan. Global Change Report N° 33. IGBP (Stockholm)